ANNALS OF GEOPHYSICS, 66, GM106, 2024; doi:10.4401/ag-8973
OPEN ACCESS

Focused and Smooth Inversion2D modelling of Magnetotelluric data from the Sabalan Geothermal Field in Northwestern Iran

Maedeh Hasanalizadeh Kolagari[1], Ali Nejati Kalateh[*,1]

(1) Faculty of Mining, Petroleum and Geophysics Engineering, Shahrood University of Technology, Shahrood, Iran

Article history: received April 27; 2023; accepted February 29, 2024

Abstract

Magnetotelluric measurements from the Sabalan geothermal field in northwestern Iran have provided clear indications of geothermal reservoirs. This study aimed to identify shallow and deeper conductivity anomalies associated with geothermal systems in the Sabalan area. The magnetotelluric method is widely used for exploring subsurface resources, as it is suitable for detecting subsurface anomalies at significant depths. Based on modeling results, thick conductive layer was found near the surface of the Moil Valley area, where two reservoirs are embedded. The main reservoir, located on the west side of Sabalan volcano, extends from the south and southwest of Sabalan peak to the west and Moil valley. The dimensions of this reservoir are almost twice as large as the estimated volume obtained from previous studies. Another smaller reservoir is located to the north of the peak.

Keywords: Geothermal; Smoothing inversion; Focusing inversion; Magnetotelluric; 2D inversion

1. Introduction

Geophysical methods, especially the magnetotelluric (MT) method, play a critical role in geothermal exploration. The MT technique is a natural electromagnetic method that measures variable magnetic and electric fields, providing information about vertical and lateral variations of the Earth's electrical resistivity structure [Cagniard, 1953; Vozoff, 1991]. Underground electrical resistivity distribution is a crucial parameter for the characterization of the geothermal systems [e.g. Muñoz, 2014]. Geothermal systems are in general composed by systems of faults and fractures filled with geothermal fluids, which can have high concentrations of dissolved salts, thus resulting in conducting electrolytes in a rock matrix. Both fluid and matrix resistivity depend on temperature, and the geothermal system exhibits, generally, higher conductivity values than the host rocks [Muñoz, 2014]. Also, clay mineral alterations resulting from the hydrothermal processes that take place in geothermal systems can dominate the high conductivity signature and can be used as a useful proxy for temperature. Brines and clays that cap a geothermal system derive from prolonged reactions of the rocks with the thermal fluids forming a clay alteration layer over a wide temperature range from less than 100°C to over 200°C [Caldwell et al., 1986]. Resistivity patterns of high-temperature geothermal systems in volcanic environment [e.g. Cumming, 2009; Cumming and Mackie, 2010; Árnason et al., 2010; Mũnoz, 2014] typically show a shallow low resistivity layer that corresponds to the clay cap made by low temperature and

low resistivity smectites with very high CEC values [e.g. Ussher et al., 2000; Lévy et al., 2018; Armadillo et al., 2019]. Below the clay cap, higher temperature stable Illite and chlorite are expected to increase the resistivity due to their lower CEC. This transition depends on temperature [about 200 °C, Ussher et al., 2000] and therefore the iso-resistivity contours may represent a proxy for the isotherms [e.g. Lévy et al., 2018; Didas et al., 2023]. Usually, MT data span a frequency range from 1 kHz to less than 0.001 Hz, corresponding to a depth range from a few tens of meters to many kilometers, allowing to completely investigate the common geothermal systems of economic interest. Although water-dominated geothermal systems have low resistivity signatures, the reverse is not always true, and additional constraints from geological and other geophysical data to limit uncertainties [e.g. Spichak and Manzella, 2009]. Inversion methods determine parameters of the model whose response is similar to the observed data. In the inverse problem, the goal is to reconstruct the model from a set of measurements. Many works use two-dimensional inversion techniques to interpret MT data, although the real earth is three-dimensional, and the two-dimensional model is assumed to be a simplification of the real structures. In 1998, a semi-detailed regional MT survey was conducted at 212 stations over the geothermal system of Sablan [KML., 1998], located on the northwest slope of Mount Sablan, a large stratified volcano in Ardabil province, northwest Iran. The Sablan geothermal system is considered a high temperature system [KML., 1998]. Three deep exploratory wells and two shallow wells were drilled between 2002 and 2004. Hence, new exploration pads, Pad D (NWS-7D) and Pad E (NWS-8D), were recommended and later constructed southeast of NWS-1D in preparation for Stage 2 drilling activities in NW Sabalan project. The review proposed a hydrological model suggesting that the up flow is more likely situated east-southeast of the Moil Valley. Hence, Pad D and Pad E were sited southeast of NWS-1D. An increasing elevation of shallow conductive layer was observed from the drilled sector to Pad D. However, a less conductive body (15 Ω-m) apparently underlies Pad E and the area immediately south of Pad E is modeled to have a resistive body from surface to bottom. At deeper level of −2300 (m.a.s.l) as shown, a conductive layer underlies the drilled area including Pad D and Pad E. The sector east of Pad D and Pad E, which is conductive at lower elevation i.e., 2600 (m.a.s.l), now exhibits increasing resistivity at depth. Profile P01 cuts across drilled wells NWS-1D and Pad D and Pad E. This profile shows that a conductive layer previously undetected by the 1998 MT survey underlies Pad E. The ~500m-thick, <14-Ωm conductive layer is modeled at depths between 200 and 500 m along the entire length of the profile and generally follows the topography of the area. The interface between the conductive layer and the resistive basement is deeper within the drilled sector at about 2000 (m.a.s.l) and shallower in the southeast at approximately 2500 (m.a.s.l). This elevation difference indicates geothermal fluids outflowing from the southeast towards Moil Valley [EDC, 2007]. Based on Tables 1 and 2 and Figure 7, significant relationships between temperature and rock layers and resistivity can be identified. As examples, the information obtained from well outputs and geological cores indicates that in the shallow layers at depths of 170 to 200 meters, temperatures are below 100 degrees Celsius. At this depth and temperature range, rocks such as Smectite, Tridymite, and Cristobalite are encountered. At a depth of approximately 960 meters, temperatures ranging from 200 to 220 degrees Celsius are observed, and rocks such as Illite and Incipient to Anhedral Epidote are encountered. In the depths of the studied area, ranging from 2100 to 2500 meters, temperatures around 220 to 240 degrees Celsius are observed, and rocks such as Illite-Smectite, Anhedral Epidote, and Laumonite are encountered. Here we have modelled the electrical resistivity variations along an approximatively 2D profile made by 9 MT stations passing through the exploratory wells. The objective is to find main reservoir by modeling the data and use geological researches.

2. Geological and geophysical setting

2.1 Location

The geothermal energy development program in Iran began in 1975, demonstrating the potential of geothermal energy in the northern part of the country. The program was temporarily suspended in 1983 and was postponed until extensive exploratory studies were defined in 1995, with a focus on the promising area in the northwestern region of Iran, Sabalan, with the aim of developing the first geothermal power station. Sabalan is a large stratovolcano, which includes a large central construction built on a possible tectonic horst of intrusive and effusive volcanic rocks, it is built upon a tectonic horst, which denotes an elevated block bounded by faults and distinguished from the surrounding areas. This horst is comprised of intrusive rocks, which are formed by the solidification of magma beneath the Earth's surface, as well as effusive volcanic rocks, which are the result of volcanic eruptions and

subsequent lava flows. Therefore, the geological structure of Sabalan showcases the interplay between tectonic processes and volcanic activity, with the central construction intricately associated with the formation and evolution of the tectonic horst.

2.2 Description of the field

Mount Sabalan is a large stratovolcano located in Ardabil province in the northwest of Iran. It is a trachyandesite massive volcano located south of the Caspian plate, near the three-way connection of the Eurasian plates, Iran, and Saudi Arabia. The relative movements of the plates, such as the rotary moving motion from the downfall down the Arabic plate below the Iranian plate, define a compact tectonic area in the region.

2.3 Main past investigations and main results

Since 1996, several potentially geothermal regions have been discovered through several projects by the Renewable Energy Organization of Iran (SUNA). For geothermal purposes, different geophysical concepts will be useful in reducing the ambiguity of both datasets and stronger concepts. In 2007 and 2009, the Exploration and Development Company (EDC) (Energy Development Corporation) conducted an MT survey at 78 locations to identify the potential resource center and determine the drilling targets for the development of geothermal energy exploration. The survey identified a promising area with high electrical resistivity and low seismic velocity, suggesting the presence of a hydrothermal system. The MT survey results have been interpreted to indicate that the geothermal system at Sabalan is primarily associated with a deep fault system. The fault system is likely to be the main pathway for the transport of geothermal fluids to shallower geological structures. Further drilling is required to confirm the presence of a commercially viable geothermal resource at Sabalan. However, the MT survey results suggest that the area is promising and further exploration is warranted. The geographic location of Sabalan with distribution of the MT stations and MT profile in Figure 1 and 2.

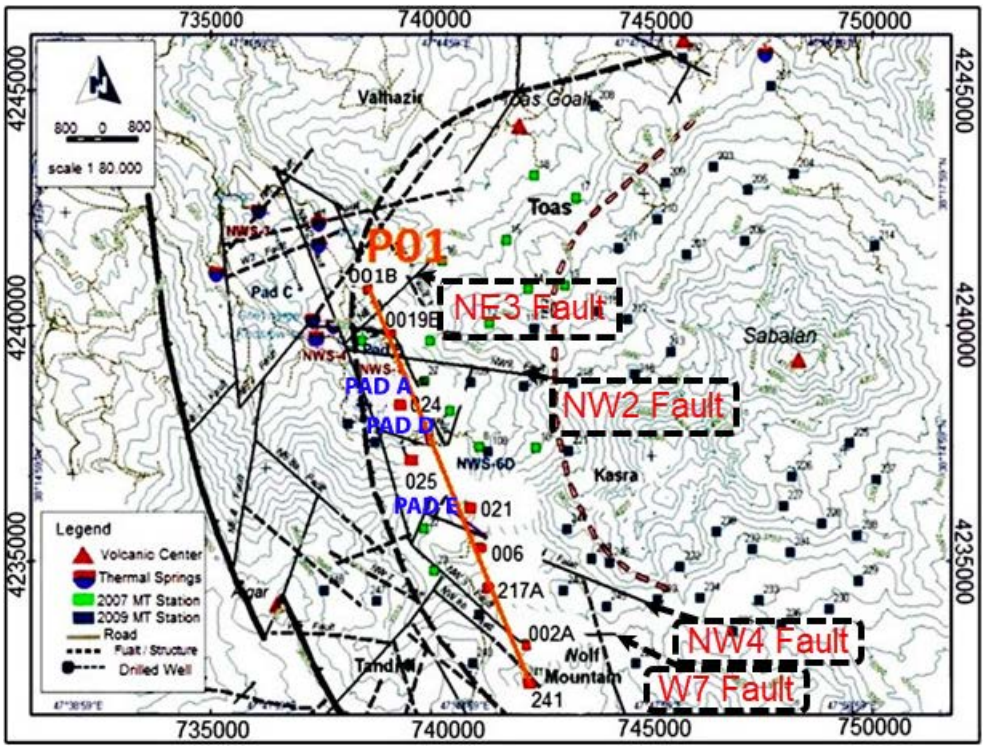

Figure 1. The geographic location of Sabalan, with distribution of the MT stations and MT profile [EDC, 2009].

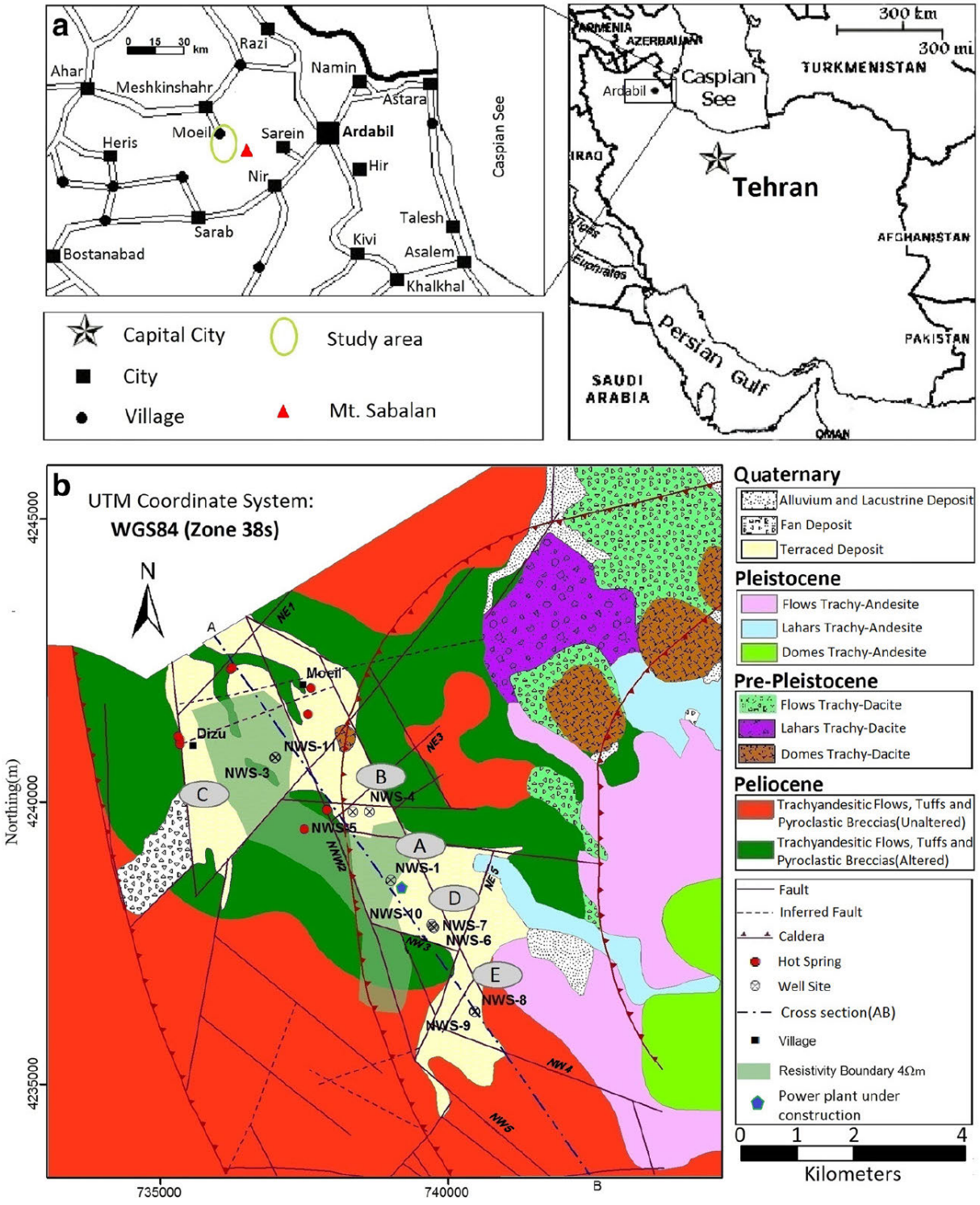

Figure 2. a) Geographical situation of study area, b) geological map of west and northwest of Mt. Sabalan (based on KML 1999a, detailed faults map is based on EDC 2010)—geothermal wells and faults are shown in bold and bold italic, respectively. The letters A, B, C, D and E on geological map represent exploration well pads [Niaraq et al., 2017].

Figure 3 describes geological feature, with NE3 being the suspected fault according to the obtained map, which can be recognized by the structure of the layers in that area. NW2, NW4, and W7 are faults that can be clearly seen on the geological map. Additionally, Pad A indicates the presence of a follow-up well to directly identify the underground layers. Pad E and Pad D are proposed wells for better access to the underground materials. Figure 4 shows the existing layers, starting with sedimentary layers and then progressing to pyroclastic and volcanics before ending with monzonites. In Pad D, these layers are divided into smectites, epidotes, and metamorphic. Smectite

and sericite layers can also be distinguished in PadE. It is important to note the distinction between the different layers and their composition in each area for further geothermal exploration and development.

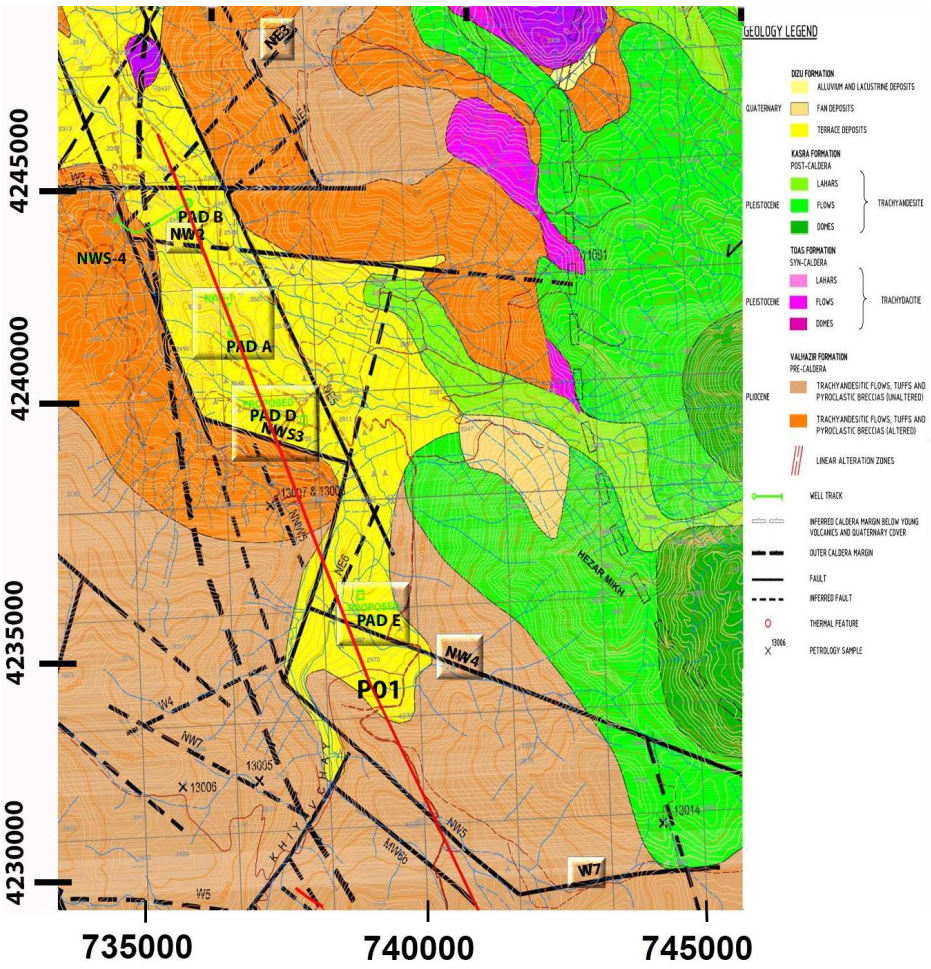

Figure 3. The geological map of Sabalan, with distribution of MT profile [SKM,2005].

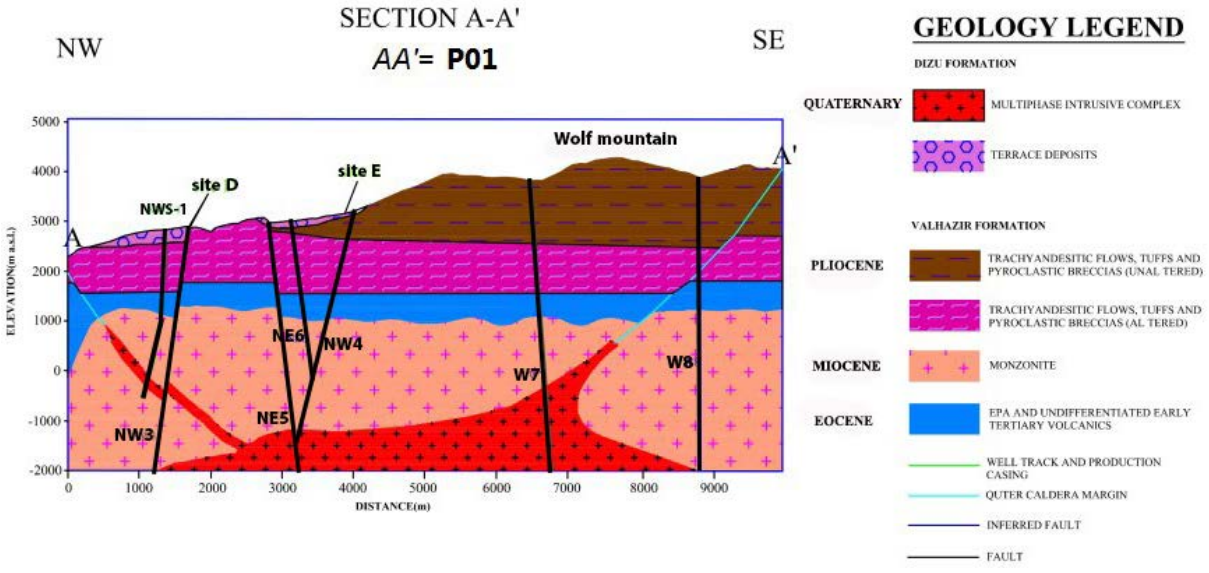

Figure 4. The geological section including the wells [SKM, 2005].

3. MT data processing and modeling

In this study, we model the existing magnetotelluric data [EDC,2009] acquired along a profile shown in Fig. 1. Data were collected using Phoenix MTU-5A data three-dimensional metering systems with a standard frequency range of 0.0005 to 380 Hz. MT data conversion from time domain to frequency domain as well as initial data editing was done using Phoenix Geophysics software Ltd.SSMT2000, and the resulting data was edited, analyzed and modeled using ZondMT2D algorithm. MT data were commonly of good quality down to 0.01 Hz [Oskooi et al., 2016].

In magnetotelluric sounding exploration, the relationship between the specific electrical components (E_x, E_y) at a specific frequency (f) and the magnetic field components (H_x, H_y) is obtained by performing a time-frequency Fourier transformation along two orthogonal directions on the earth. This technique is useful in providing a complete understanding of the subsurface electrical conductivity distribution, which can be used to infer geological structures and identify potential geothermal reservoirs.

$$E_x = Z_{xx}H_x + Z_{xy}H_y, \quad E_y = Z_{yx}H_x + Z_{yy}H_y \tag{1}$$

In the equations we mentioned:

- E_x and E_y represent the electric field in the x and y directions, respectively.
- H_x and H_y represent the magnetic field in the x and y directions, respectively.
- Z_{xx}, Z_{xy}, Z_{yx} and Z_{yy} represent impedance parameters.

In 2D analysis and modelling, it is necessary to rotate the impedance tensor Z along the two directions parallel and perpendicular to the profile. Following this rotation, the relationship between the rotated impedance tensor Z_θ and the original tensor Z is given by:

$$Z = \begin{pmatrix} z_{xx} & z_{xy} \\ z_{yx} & z_{yy} \end{pmatrix}, \qquad Z_\theta = R(\theta)ZR(\theta)^T, \qquad R(\theta) = \begin{pmatrix} \cos\theta & \sin\theta \\ -\sin\theta & \cos\theta \end{pmatrix} \tag{2}$$

where $R(\theta)$ is the rotation matrix, $R(\theta)^T$ is the transpose of the rotation matrix, and θ is the rotation angle [Ali-Yong Li et al., 2010].

MT frequency domain data is transformed into a two-dimensional geoelectric model using the nonlinear conjugate gradient (NLCG) inversion code of Rodi and Mackie [2001]. This algorithm minimizes the Tikhonov regularization function and solves for a smooth model that matches the MT data. Tikhonov [1977] defined a regularized solution to the MT inverse problem as finding the model m that minimizes the objective function (see Equation 3):

$$\psi(d - F(m))^T \vartheta^{-1}\big(d - F(m)\big) + \tau\|L(m - m_0)\|^2 \tag{3}$$

Here, d is the vector of observed data, F is the forward modeling operator, m is the unknown model vector, ϑ^{-1} is the error covariance matrix, L is a linear operator, m_0 is the reference model, and τ is the user-defined adjustment parameter.

The first term $\big(\psi\big(d - F(m)\big)^T \vartheta^{-1}\big(d - F(m)\big)\big)$ measures the mismatch between the observed data and the modeled data, while the second term $(\tau\|L(m - m_0)\|^2)$ measures the smoothness of the model and its proximity to the reference model. The degree of smoothness is controlled by the parameter τ, [Wen Xiao ,2004].

The relationship between the data and model parameters in an inversion method can be expressed as $(d = G(m))$, where d is the data vector of length N, G is the nonlinear forward model, and m is the vector of model parameters. The Occam's smooth inversion method was introduced by Constable and his colleagues [1987], in which an objective function is minimized to fit the data using the least squares method. This can be expressed mathematically as follows:

$$\min \varphi_m = \|W_m m\|^2 \tag{4}$$

φ_d providing $\left\|W_d\left(d^{obs}-G(m)\right)\right\|^2$ will be $\varphi_d{}^*$:

$$\varphi_d = \left\|W_d(d^{obs}-G(m))\right\|^2 = \varphi_d{}^* \tag{5}$$

where m is the vector of the unknown parameters of the problem, W_m is the weighting matrix of the model parameters, W_d is the weighting matrix of the data, which is a diagonal matrix containing the inverse of standard deviation of each datum, d^{obs} is the vector of the collected data and $\varphi_d{}^*$ is the desired misfit value; Therefore, it can be said that an optimization problem has been encountered for which a general objective function has been considered as follows:

$$\Phi = \left\|W_d(d^{obs}-G(m))\right\|^2 + \beta^2\|W_m m\|^2 \tag{6}$$

β is the balance parameter that determines the degree to which each term is minimized. To obtain the model, the general objective function is minimized, by taking the derivative Φ with respect to m and setting it equal to zero ($\frac{\partial\Phi}{\partial m}=0$). On the other hand, forward operator G is completely nonlinear. Therefore, solving the relationship $\frac{\partial\Phi}{\partial m}=0$, becomes very complicated. In order to be able to solve $\frac{\partial\Phi}{\partial m}=0$, the forward model must be locally linearized Taylor expansion G around a known model using a Taylor series and removing high-order derivatives. Suppose the model m^k is known in the kth iteration.

The parameters of the model m^{k+1} in each iteration are given by:

$$m^{k+1} = \left[J(m^k)^T W_d^T W_d J(m^k) + \beta^2 W_m^T W_m\right]^{-1} J(m^k)^T W_d^T W_d^{\tilde{d}}(m^k) \tag{7}$$

Equation (7) is the final equation of the smooth inversion method. The iteration process starts with an initial model, and the calculated model gets closer to the main model in each iteration until it reaches the desired model.

Focused inversion is a geophysical modeling method used to process geophysical data. In this method, the geophysical information received from the field, as well as data from other sources, are processed preliminarily to remove fluctuations in the signals. The focused inversion process then utilizes an algorithm called ZondMT2D to solve equations related to modeling. The algorithm includes equations related to electric current density, electric potential, magnetic field, and electrical conductivity coefficient of the earth. ZondMT2D aims to create the best possible model of the subsurface, taking into account adjustable parameters such as depth, electrical conductivity coefficient, slope, and height shape of the layers. The Focused Inversion method provides compact and simple structural models by minimizing a proper function of resistivities. Initially, the weight matrix is set to the identity matrix, which means that the method starts with the least squares solution. Next, a weighting function is calculated and used in the least square inversion to increase the compression of the model. According to this method, the iterative procedure stops when the minimum area of the model is reached [L. Ekinci et al., 2008]. The Focused Inversion method utilizes the least squares method with a smooth operator and additional contrast focusing. This algorithm can produce a distribution of smooth piecewise parameters, which is a model that contains constant resistivity blocks. The algorithm is sensitive to the threshold parameter, which determines whether adjacent cells are unified or not. If the contrast of adjacent cells is higher than the specified value, the cell parameters are averaged weakly, if lower, strongly. The matrix equation for this inversion type is given as Equation (8) [Zond geophysical software Saint-Petersburg., 2001-2012]:

$$(A^T W^T W A + \mu C^T R C)\Delta m = A^T W^T \Delta f - \mu C^T R C m \tag{8}$$

where A is the Jacobian matrix of partial derivatives, C is the smoothing operator, W is the relative error matrix, m is the section parameters vector, μ is the regularizing parameter, Δf is the discrepancy vector between observed and calculated values and R is the focusing operator.

In this project, a comparison is made between smooth inversion and focused inversion along a significative profile where independent information derived from geological observation and exploration wells and logs are available. Figures 5 and 6.

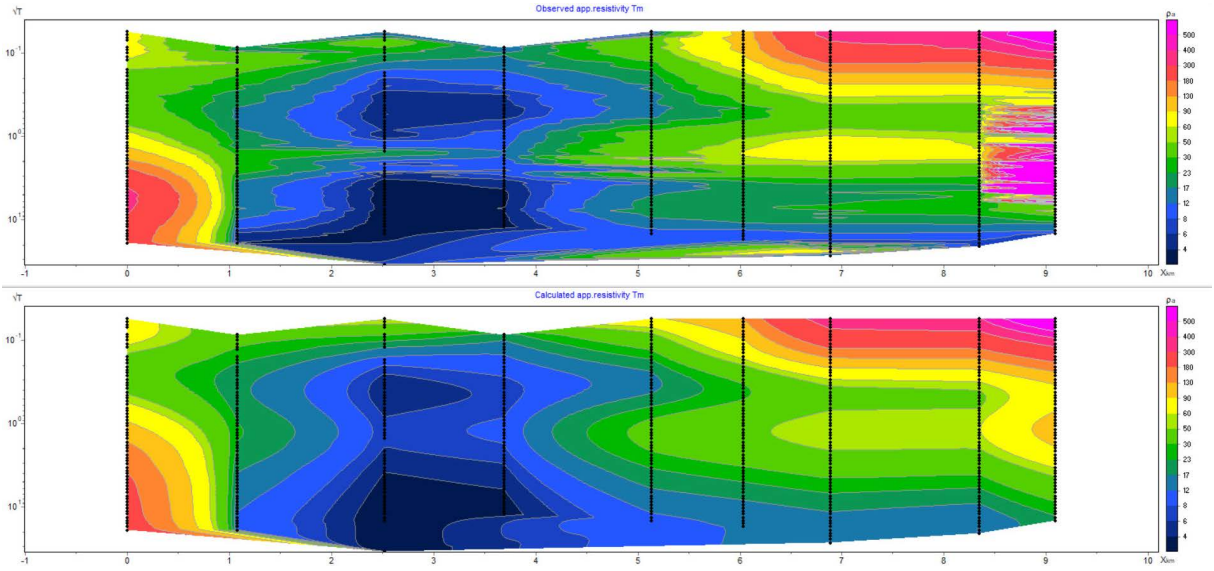

Figure 5. Focused inversion pseudo section.

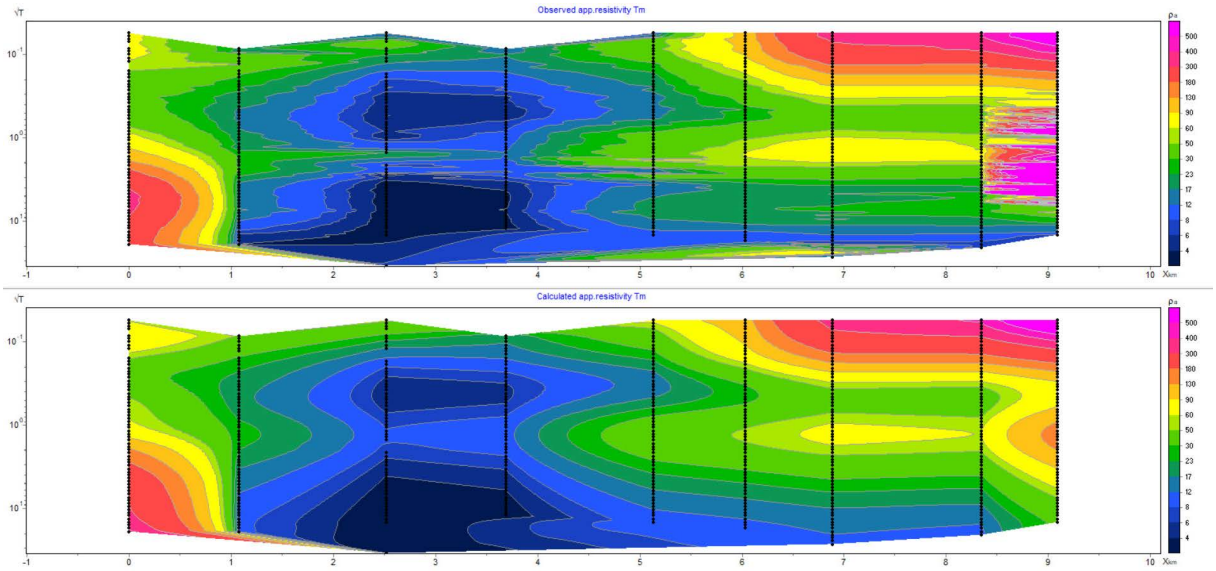

Figure 6. Figure 6.Smoothed inversion pseudo section.

3.1 Description of the smoothing inversion model

In the study area has a lot of faults, in this case, because the geothermal structure is controlled by faults, we expect very sharp changes, so smoothing inversion models are not acceptable (Figure 7).

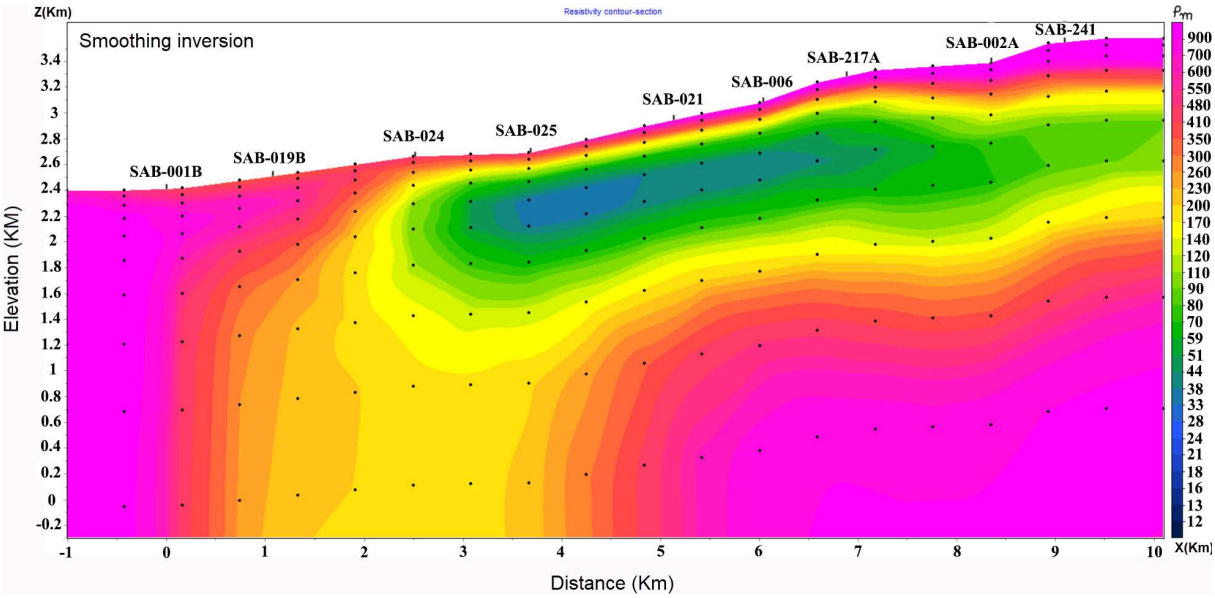

Figure 7. Two-dimensional smooth inversion of P01, RMS error 0.08.

3.2 Description of the resistivity focusing inversion model

In this resistance model, we can reach the following results. In general, this model starts with a layer with high resistance from the surface until a certain depth with a thickness of 600 meters, continues, after that a layer with very low resistivity is visible, which gives the possibility of an altered layer as a clay cab, with 1000 m thickness then from this conductive layer with low resistivity, the material of the layers is Smectite and Illit-Smectite, The layers start to increase in resistivity, and we can consider this layer with high resistivity as the main reservoir. The faults are marked on the model. Figure 8.

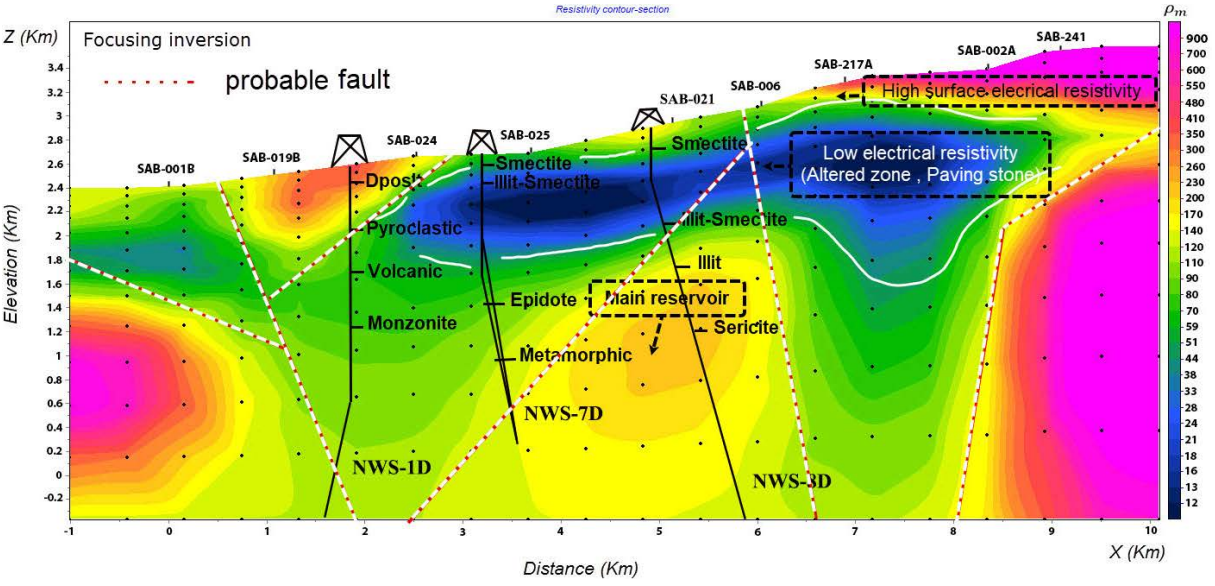

Figure 8. Two-dimensional focused inversion of P01, RMS error 0.12.

4. Interpretation from inverse modeling of MT data

The two-dimensional inversion models of the TM-mode data along profile P01 are shown in Figure 9.

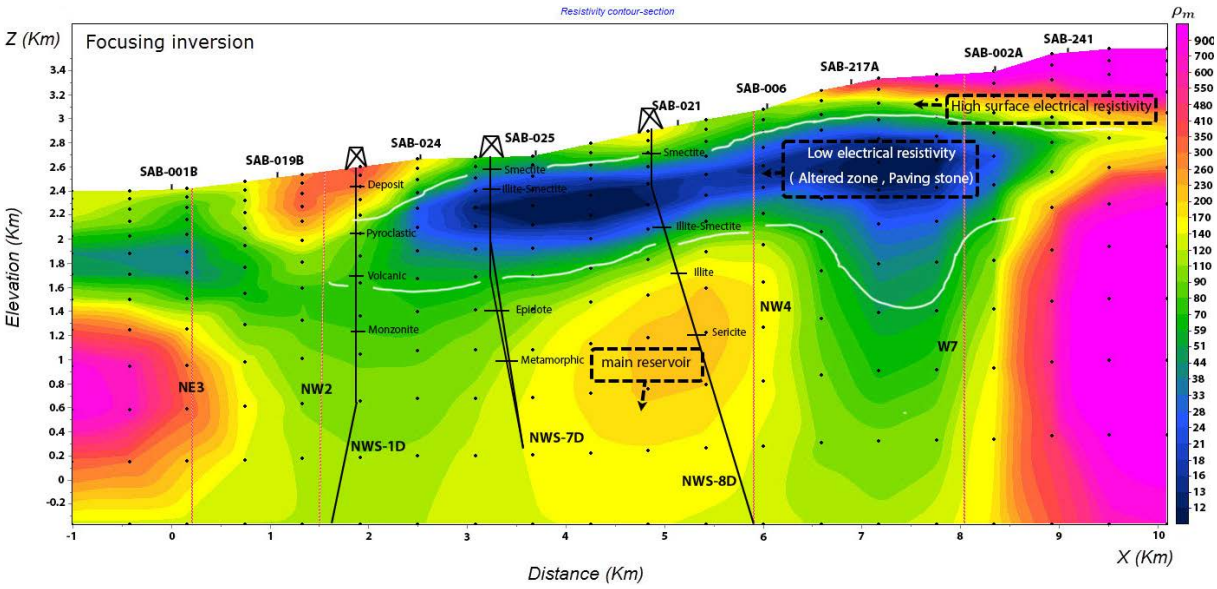

Figure 9. Two-dimensional focused inversion of P01 with geological complications, RMS error 0.12.

4.1 Descriptions of anomalies

The resistivity of the top layer varies from 50 to more than 250 Ωm as shown in Fig. 6. An anomalous conductive layer extending from the Moil valley Moil valley (that is in the North and North-West of the profile P01, figure 11) to boreholes NWS-7D and NWS-8D was observed at about 1000 (m.a.s.l) This conductive layer has a thickness of about 500-1000 m and are underlain by a moderately resistive layer of less than 50 up to 250 Ωm (Figure 9). The conductive zone less than 20 Ωm discovered within MT. Sabalan between elevations of 3000 and 2800 (m.a.s.l) is a symptom of hydrothermal activity in the region. The thickest conductive layers are commonly found in the areas of volcanic activity. The authors have concluded that the detection of geothermal reservoirs using the MT method is only marginally effective due to the likely resistivity contrasts, resolution, and measurement error levels. According to profile P01, the thickness of the conductive zones beneath pad D is between 600 m and 1000 m.

4.2 Relationships between alteration and resistivity

In the upper levels of active geothermal systems (temperatures < 200 °C) where low salinity groundwaters or mixed groundwater-geothermal fluids are present, the lowtemperature, high-CEC smectite clays will dominate over the fluid salinity as the main pathway for conduction. At deeper levels in the systems where higher salinity fluids occur and lower CEC illites prevail, clay conductivity will be less of s fsctor [Ussher et al., 2000, Cumming, 2009; Cumming and Mackie, 2010; Mũnoz, 2014; Armadillo et al., 2020, Rizzello et al., 2022]. Figure 10.

Furthermore, the relevance with the NWS-7D well data (see Table 1) indicates that the conductive layer coincides with the smectite (Sm) and Illite-Smectite (Ill-Sm) zones, while the epidote zone corresponds to increasing resistivity values (more than 30 Ωm). By correlating different alteration mineral assemblages with resistivity, it was found that pure Illite and epidote are two higher temperature minerals that have resistivity values of more than 20 Ωm. Based on the NWS-8D well data (see Table 2), the Sm, Chlorite (Cl), and Ill-Sm zones are present within less than 30 Ωm, while the presence of Illite and Sericite coincides with more than 30 Ωm. Further correlation reveals that the Paleozoic Metamorphic is located within layers with more than 70 Ωm resistivity.

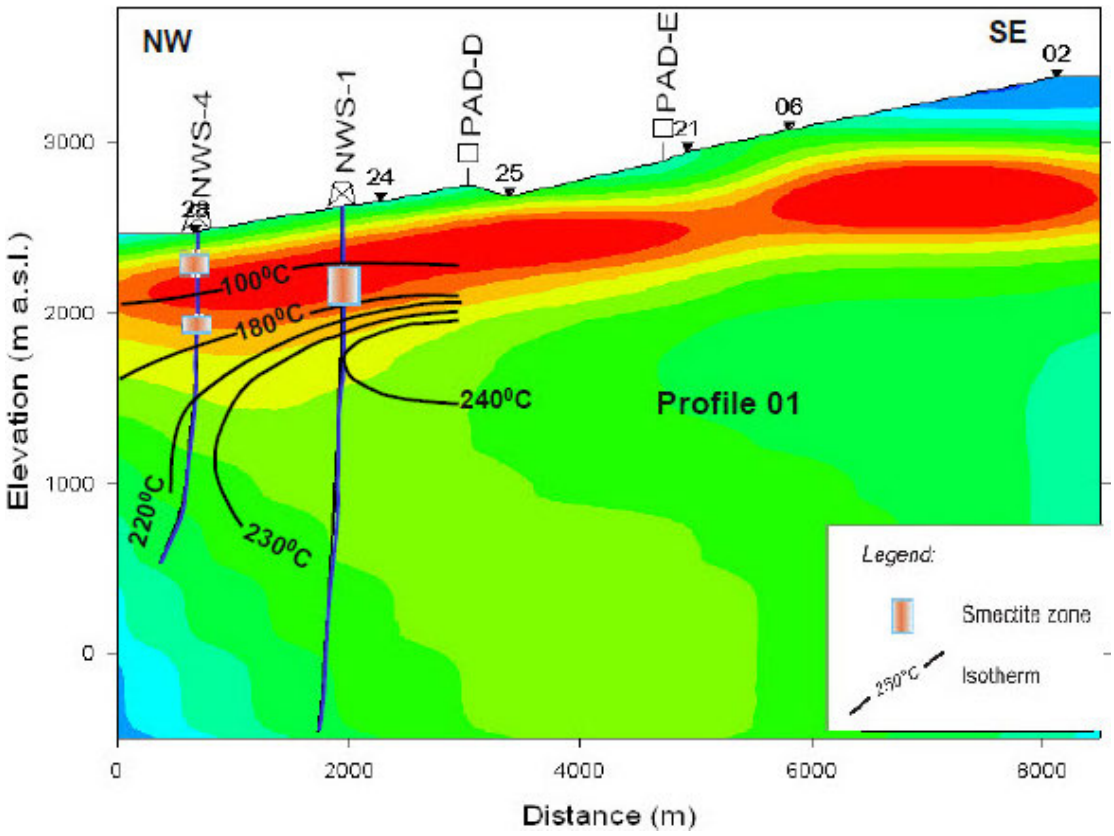

Figure 10. Corelation of resistivity model with temperature and distribution of Smectite zone in wells [EDC, 2008].

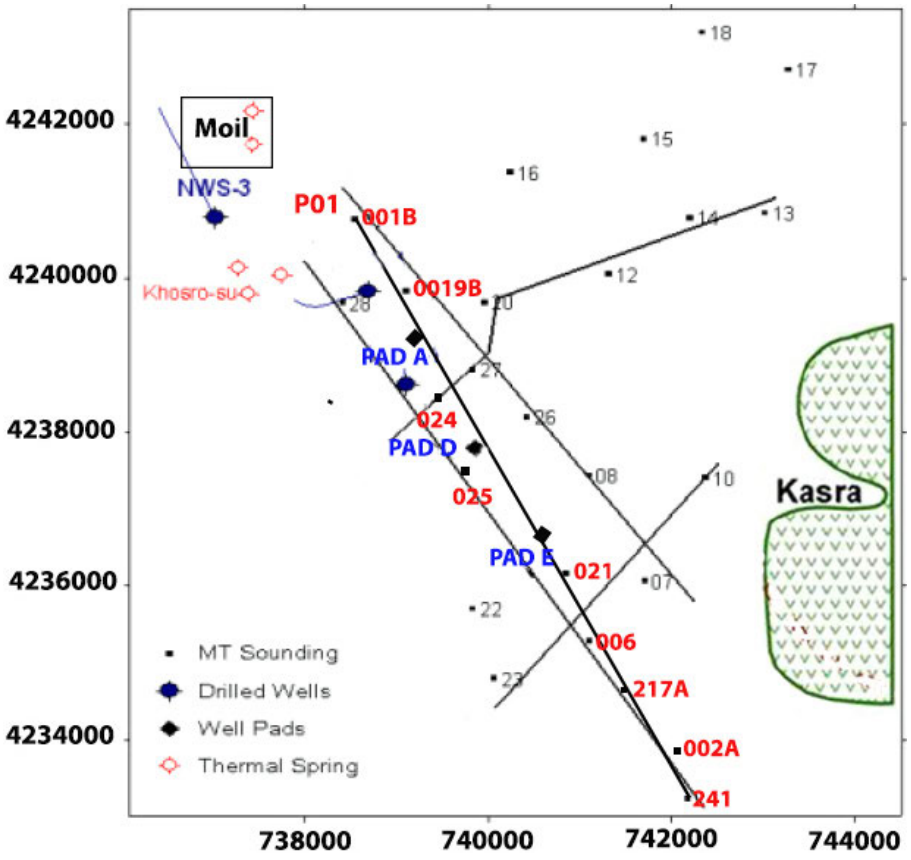

Figure 11. Profile lines [EDC, 2008].

Depth [m MD/m VD]	Predicted Temperature [°C]	Index Minerals
~ 200	<100	Smectite, Tridymite, Cristobalit
~420	~120	Chlorite, Smectite
~550	~150-180	Illite-Smectite, Quartz
~820	~180-200	Incipient Epidote
~960	~200-220	Illite, Incipient to anhedral Epidote
1316/1280	~240-250	Euhedral to Subhedral Epidote
2180/1982	≤250	Euhedral to subhedral Epidote veins
2480/2188	~220-240	Illite-Smectite, anhedral Epidote, Laumonite
2700/2260	~220-240	Laumonite

Table 1. Alteration mineral geothermometers and predicted temperatures, borehole NWS-7D [EDC, 2008].

Depth [m MD/m VD]	Predicted Temperature [°C]	Alternation Mineral Geo-Thermometers
170	<100	Smectite, Tridymite
280	~120	Chlorite, Sphene
300-486	~120-150	Illite-Smectite Smectite, Vermiculite, Chlorite
495-696	~150-180	Incipient to anhedral Epidote Illite-Smectite, Quartz
706-958	~180-200	Illite-Smectite, Incipient to anhedral Epidote
1251	200	Illite-Smectite, anhedral Epidote
1624	~250	Illite-Smectite, Anhydrite, Sericite
1743	~250	Epidote, Illite, Chlorite
1785	~250-260	Vein Epidote, Illite, Chlorite
1815	~260	Actinolite, Biotite, vein Epidote
2174	≤260	Muscovite, Illite, Biotite, Epidote
2341	~260-280	Muscovite, Andalusite

Table 2. Alteration mineral geothermometers and predicted temperatures, borehole NWS-8D [EDC, 2010].

4.3 Relationships with temperature distribution

Also, to be examined the presence of the shallow conductive layer that is usually interpreted as the clay cap made by low temperature and low resistivity smectites with very high cation exchange capacity (CEC) values [Ussher et al., 2000; Cumming, 2009; Cumming and Mackie, 2010; Mūnoz, 2014; Armadillo et al., 2020, Rizzello et al., 2022]. A common conceptual model for high-enthalpy geothermal systems with magma penetrating into shallower crustal levels is the presence of a high-conductivity subsurface layer beneath an increasing resistivity layer. This resistivity distribution is also observed in the study area, where volcanic features like the Kasra dome (It is in East and South-East of the profile P01, Figure 11) may be related to an intrusive body. Additionally, the study confirmed the existence of a hotter area east of pad D, which acts as a heat source for the northwest Sablan geothermal reservoir. The height of this hotter area is about 1500 to 2000 meters from the base of the smectite clay zone with low resistivity near Kasra dome. This hotter area could be one of the local intrusion sites associated with the Mount Sablan volcanic complex and the heat source for the northwest Sablan geothermal reservoir.

4.4 Faults in the resistivity section

In the discussion take into account that in some systems there is a clear electrical resistivity signature directly associated with fault systems. For instance, in the Chingshui geothermal field [Chang et al., 2014] located in the Ilan Plain (Northeast Taiwan) and connected to the Okinawa Trough back arc basin, the main fault systems are associated with conductive anomalies and high temperatures (>140 °C) revealed by core logs. On the contrary, in other systems the faults signature in the MT resistivity models have only an indirect signature. For instance, in the geothermal systems along the Kenya rift by Lichoro et al. [2017, 2019*, in the Mbaka system [Rizzello et al., 2022] in southern Tanzania or at Alalobeda in northern Ethiopia [Rizzello et al., 2021], where faults are revealed in the resistivity MT models by vertical shifts of the bottom of the shallower conductive layers (usually associated with low temperature clay alterations) and eventually confirmed by the gravimetric signatures. In our study area resistance and temperature changes have been created in the study area due to faults. Due to the specific resistance, the changes are very intense, that is, the young volcanic layers are faulted and due to these faults, hydrothermal vapors find their way to the surface. In the flow path of these vapors, due to high temperature and chemical structure, they make changes in their path, which leads to the production of clay and the creation of clay caps, which in our study area, these clay changes include Smectite, Illite-Smectite, and Illite. Figures 8 and 9.

5. Conclusion

According to the modeling of the studied area, we come to the conclusion that the layers with high resistance start from the surface and continue in areas with a low thickness of about 200 (m) to areas with a greater thickness of about 600 (m). With the process of decreasing resistance, this layer reaches a layer with a very low resistance of 10 to 30 (ohm meters), which is considered as our clay layer, which can be one of the signs of the existence of our main geothermal source in this area. In this study, this layer also has a variable thickness, it is from 300 to 1000 (m). Then this layer begins to increase in resistance by increasing the depth, which is considered as the main reservoir for the geothermal source. Two-dimensional inversion generates specific resistance cross-sections, which, when combined with exploratory well and borehole data and geological investigations, reveal that evidence of the Sablan geothermal system is consistent with that found by Johnston et al., [1992], wherein thick conductive layers were identified on the outer edge of the reservoirs. According to interpretation, resulting from two-dimensional modeling of MT data, the main reservoir is located on the western side of Sablan, extending to the west and Moil Valley, from the south and southwest of the peak. Another area with greater heat was also identified in the east of Pad D, which may be associated with intrusive masses and could serve as a source of heat for the northwest Sablan geothermal project.

References

Armadillo E., D. Rizzello, C. Pasqua, P. Pisani, A. Ghirotto, K. Kabaka, T. Mnjokava, J. Mwano, L. Didas, L. Tumbu (2020). Geophysical constraints on the Luhoi (Tanzania) geothermal conceptual model, Geothermic, 87, 101875.

Bromley et al. (2000). Geophysical Exploration of Sabalan Geothermal Prospects In Iran. Proceedings World Geothermal Congress 2000, Kyushu-Tohoku, Japan, May 28 – June 10, 2000.

Cumming, W. (2009). Geothermal resource conceptual models using surface exploration data. In: Proceedings of the Thirty-Fourth Workshop on Geothermal Reservoir Engineering. Stanford University, Stanford, California, February 9-11, 2009.

Cumming, W., R. Mackie (2010). Resistivity imaging of geothermal resources using 1D, 2D and 3D inversion and TDEM static shift correction illustrated by Glass Mountain Case History. In: Proceedings of the World Geothermal Congress. Bali, Indonesia, April 2010, 25-29.

Constable, S.C., R.L. Parker and C.G. Constable (1987). Occam's inversion, A practical algorithm for generating models from electeromagnetic sounding data, Geophysics., 52, 289-300.

Emami, M.H (1994). 1:100,000 geological map of Iran, Sheet 5566. Ministry of Mines and Metals, Geological Survey of Iran, Tehran, Iran.

Energy Development Corporation (EDC) (2008, 2007). MT survey of NW Sabalan geothermal project, NW Iran. Report submitted to the SUNA, 19.

Energy Development Corporation (EDC) (2010, 2009). MT survey of NW Sabalan geothermal project, NW Iran. Report submitted to the SUNA, 13.

Fitterman, D.V. and R.F Corwin (1982). Inversion of self-potential data from the Cerro Prieto geothermal field, Mexico, Geophysics, 47, 938-945.

Ghaedrahmati et al. (2013). 3-D inversion of MT data from the Sabalan geothermal field, Ardabil, Iran, J. Applied Geophys. 93, 2023, 12-24.

Hanano, M. (2000). Two different roles of fractures in geothermal development. In: Proc. World Geothermal Congress 2000, Kyushu-Tohoku, Japan, 597-2602.

Johnston, J.M., L. Pellerin and G.W. Hohmann (1992). Evaluation of electromagnetic methods for geothermal reservoir detection. Geotherm. Res, Council Trans., 16, 241-245.

KML (Kingston Morrison Limited Co.) (1998). Sabalan geothermal project, Stage 1 – Surface exploration, final exploration report, Kingston Morrison Limited Co., report 2505-RPT-GE-003 for the Renewable Energy Organization of Iran, Tehran, Iran, 83.

Khojamli, A., F. Doulati Ardejani, A. Moradzadeh, A. Nejati Kalate, A. Roshandel Kahoo and S. Porkhial (2017). Determining fractal parameter and depth of magnetic sources for Ardabil geothermal area using aeromagnetic data by de-fractal approach. J. Mining Environ., 8,1, 93-101

Levent Ekinci, Y. and A. Demirci (2008). A Damped Least-Squares Inversion Program for the Interpretation of Schlumberger Sounding Curves, J. Applied Sci. 8, 22, 4070-4078.

Lévy, L., B. Gibert, F. Sigmundsson, Ó.G. Flóvenz, G.P. Hersir, P. Briole, P.A. Pezard (2018). The role of smectites in the electrical conductivity of active hydrothermal systems: electrical properties of core samples from Krafla volcano, Iceland, Geophys. J. Int. 215, 1558-1582, https://doi.org/10.1093/gji/ggy342.

Montahaei and Ghanbarifar (2020). A comparison of regularized, sharp boundary and tear zone inversions along an MT profile in Sabalan geothermal field, Iran. E3S Web of Conferences 211, 02004 (2020) The 1st JESSD Symposium 2020.

Mũnoz, G. (2014). Exploring for geothermal resources with electromagnetic methods, Surv. Geophys. 35, 101-122, https://doi.org/10.1007/s10712-013-9236-0.

Noorollahi, Y. and R. Itoi (2011). Production capacity estimation by reservoir numerical simulation of northwest (NW) Sabalan geothermal field, Iran. Energy 36, 7, 4552-4569.

Oskooi, B., L.B. Pedersen, M. Smirnov, K. Arnason, H. Eysteinsson, A. Manzella and the DGP Working Group (2005). The deep geothermal structure of the Mid-Atlantic Ridge deduced from MT data in SW Iceland, Phys. Earth Planet. Inter., 150, 183-195.

Oskooi, B., M. Takalu, M. Montahaei and M.R. Rahmani (2016). A recent magnetotelluric investigation of the Sabalan geothermal field in north-western Iran, Boll. Geofis. Teor. Appl., 57, 3, 261-274.

Rizzello, D., E. Armadillo, C. Pasqua, P. Pisani, R. Balsotti, S. Kebede, A. Mengiste, Y. Kebede, G. Hailegiorgis, K. Mengesha (2021). The geophysical recognition of a vapor-cored geothermal system in divergent plate tectonics: the Alalobeda (Alalobad) field Ethiopia., Tectonophys 813, 228933.

Rizzello, D., E. Armadillo, C. Pasqua et al. (2022). Assessment of the Kiejo-Mbaka geothermal field by three-dimensional geophysical modelling, Geomech. Geophys. Geo-energ. Geo-resour., 8, 143.

Seyedrahimi-Niaraq et al. (2017). Development of an updated geothermal reservoir conceptual model for NW Sabalan geothermal field, Iran, Geotherm Energy 5, 14, doi:10.1186/s40517-017-0073-0.

Seyedrahimi-Niaraq et al. (2019). A three-dimensional numerical model to simulate Iranian NW Sabalan geothermal system, Geothermics, 77, 42-61.

Spichak, V. and A. Manzella (2009). Electromagnetic sounding of geothermal, J. Appl. Geophys., 68, 459-478.

Talebi, B. (2006). Numerical modeling of the NW SABALAN geothermal field, IRAN, Proceedings, Thirty-First Workshop on Geothermal Reservoir Engineering, Stanford University, Stanford, California, January 30-February 1, 2006, SGP-TR-179.

Tikhonov, A.N. and V.Ya. Arsenin (1977). Methods of solution of ill-posed problems, New York,Wiley.

Ussher, G., C. Harvey, R. Johnstone, E. Anderson (2000). Understanding the resistivities observed in geothermal systems. In: Proceedings of the World Geothermal Congress 2000. Kyushu-Tohoku, Japan, May 28 – June 10, 2000.

Vozoff, K. (1991). The magnetotelluric method in Electeromagnetic Methods in Applied Geophysics, M.N. Nabighian, Ed. SEG, Tulsa, 2, 8, 713-809.

Xiao, W. (2004). Ms Thesis, Magnetotelluric exploration in the Rocky Mountain Foothills, University of Alberta, Edmonton, Canada.

Zarei et al. (2015). Geochemistry and Alteration Mineralogy of Well NWS-10, Mt. Sabalan Geothermal Field, NW-Iran, GRC Transactions, 39, 2015.

Zond geophysical software, Saint-Petersburg, (2001-2012).

***CORRESPONDING AUTHOR: Ali Nejati KALATEH**,
Faculty of Mining, Petroleum and Geophysics Engineering, Shahrood University of Technology, Shahrood, Iran
e-mail: nejati@shahroodut.ac.ir